REVIEW

doi:10.1038/nature11115

Electrocatalyst approaches and challenges for automotive fuel cells

Mark K. Debe[1]

Fuel cells powered by hydrogen from secure and renewable sources are the ideal solution for non-polluting vehicles, and extensive research and development on all aspects of this technology over the past fifteen years has delivered prototype cars with impressive performances. But taking the step towards successful commercialization requires oxygen reduction electrocatalysts—crucial components at the heart of fuel cells—that meet exacting performance targets. In addition, these catalyst systems will need to be highly durable, fault-tolerant and amenable to high-volume production with high yields and exceptional quality. Not all the catalyst approaches currently being pursued will meet those demands.

The current performances of the small test fleets of vehicles powered by automotive fuel cells are impressive, reflecting 15 years of intense development of all aspects of proton exchange membrane (PEM) fuel cells that have brought the technology close to pre-commercial viability[1]. But to move towards a genuinely practical technology that can be mass-produced cost-effectively, important further improvements are needed. This calls for a critical look at how we need to develop key components determining fuel-cell performance, durability and cost. A pivotal component is the electrocatalyst system that underpins fuel-cell operation, and excellent reviews of progress made in Pt-based fuel-cell catalyst development for automotive applications have been written from both an academic perspective focused on fundamentals and from a perspective focused on the requirements of the automotive companies[2–6]. This review is provided from the perspective of a fuel-cell component supplier who needs to consider all factors that any electrocatalyst approach will need to meet if it is to be commercially successful. Following an overview of fuel cells and the challenges they need to meet for commercialization, I will consider the electrocatalyst system and the different approaches taken to ensure its performance meets automotive fuel-cell requirements. In my view, focusing only on catalytic activity targets will not be sufficient to meet the challenge posed by large-scale automotive fuel-cell commercialization, which requires the manufacture of catalyst electrodes at high rates, high quality and low costs.

Fuel-cell components

An automotive fuel cell produces electricity from the electrochemical oxidation of hydrogen. It is manufactured as a stack of identical repeating unit cells comprising a membrane electrode assembly (MEA) in which hydrogen gas (H_2) is oxidized on the anode and oxygen gas (O_2) is reduced on the MEA cathode, all compressed by bi-polar plates that introduce gaseous reactants and coolants to the MEA and harvest the electric current (Fig. 1). The electrochemical reactions occur in the MEA electrodes, each attached to a solid polymer ion exchange membrane that conducts protons but not electrons. The cathode oxygen reduction reaction (ORR) and anode hydrogen oxidation reaction both occur on the surfaces of platinum (Pt)-based catalysts. Pure water and heat are the only byproducts. Porous gas diffusion layers transport reactants and product water between the flow fields and catalyst surfaces while exchanging electrons between them.

The challenges for commercialization

Fuel-cell MEAs must meet three major criteria: cost, performance and durability. The cathode ORR is six or more orders of magnitude slower than the anode hydrogen oxidation reaction and thus limits performance, so almost all research and development focuses on improving the cathode catalysts and electrodes. Most MEA catalysts used today are based on Pt (in the form of nanoparticles dispersed on carbon black supports), with the high price of this scarce precious metal having a decisive impact on costs. Fuel-cell vehicles in the test fleets monitored by the United States Department of Energy (DOE) have used 0.4 mg of Pt per square centimetre (mg Pt cm^{-2}) or more on the cathode, and in these vehicles the catalyst/MEA stability has still been short of the 5,000-hour durability target[7]. How to reduce costs by reducing cathode loadings to <0.1 mg Pt cm^{-2} without loss of performance or durability is the subject of most electrocatalyst research. Current US DOE 2017 targets[1] for electrocatalysts aim for a total (anode + cathode) platinum group metals (PGM) loading of 0.125 mg cm^{-2} on MEAs able to produce rated stack

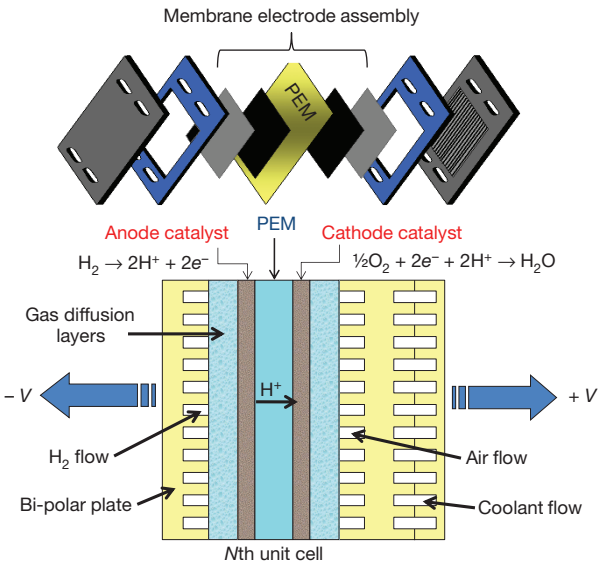

Figure 1 | Fuel-cell components. Unit cell cross-section of the *N*th unit cell in a fuel-cell stack, showing the components of an expanded MEA.

[1]3M Fuel Cell Components Program, 3M Center, St Paul, Minnesota 55144, USA.

Table 1 | Development criteria for automotive fuel-cell electrocatalysts

Performance	• Must meet beginning-of-life performance targets at full and quarter power. • Must meet end-of-life performance targets after 5,000 h or 10 years operation. • Must meet performance, durability and cost targets and have less than 0.125 mg PGM per cm^2. • Corrosion resistance of both Pt and the support must withstand tens of thousands of start-up/shut-down events. • Must have low sensitivity to wide changes in relative humidity. • Must withstand hundreds of thousands of load cycles. • Must have adequate cool start, cold start and freeze tolerance. • Must enable rapid break-in and conditioning (the period needed to achieve peak performance).
Materials	• Must have high robustness, meaning tolerance of off-nominal conditions and extreme-load transient events. • Must produce minimal H_2O_2 production from incomplete ORR. • Must have high tolerance to external and internal impurities (for example, Cl^-) and ability to fully recover. • Must have statistically significant durability, meaning individual MEA lifetimes must enable over 99.9% of stacks to reach 5,000-hour lifetimes. • Electrodes must be designed for cost-effective Pt recycling. • Environmental impact of manufacturing should be minimal at hundreds of millions of square metres per year.
Process	• Environmental impact must be low over the total life-cycle of the MEAs. • Manufacturing rates will need to approach several MEAs per second. • MEA manufacturing quality must achieve over 99.9% failure-free stacks at beginning of life (one faulty MEA in 30,000 for just 1% stack failures). • Proven high-volume manufacturing methods and infrastructure will be required. • Catalyst-independent processes will be preferred, to enable easy insertion of new-generation materials.

power densities of 8.0 kW g^{-1} Pt. This gives 8 g of PGM per vehicle, similar to what is in an internal combustion engine today.

Vehicle operation imposes severe durability and performance constraints on the fuel-cell cathode electrocatalysts[1] beyond the fundamental requirement for high ORR activity. System integrators require that the MEA produce at least 0.6 V at 1.5–2 A cm^{-2} owing to radiator size and related cooling constraints. Catalysts must survive hundreds of thousands of load cycles and tens of thousands of start-up and shut-down events over the 5,000-hour lifetime of the stack[1]. Although durability is beyond the scope of this review, serious degradation is associated with the tendency for the cathode to reach potentials above the onset of oxidation of carbon in contact with Pt, during even the short times when H_2/air waves move through the flow fields during start-up or shut-down[8]. Some of the countermeasures being developed are using more stable graphitized carbon, using catalyst supports that will not electrochemically corrode, and adding oxygen evolution catalysts to the mix to clamp the potentials at the start of water oxidation[9,10]. Table 1 summarizes these major catalyst requirements, along with secondary criteria and manufacturing considerations.

Some fundamental electrochemical considerations

MEA performance is reflected in its polarization curve, a plot of cell voltage versus current density (Fig. 2). As current is drawn from a cell, its voltage decreases as a result of three primary sources of power loss: ORR kinetic losses of the cathode, current times resistance (iR) losses due to material and interface resistances, and mass transport overpotentials at high current densities when it is difficult for the catalyst to get enough oxygen from air. For the polarization curve conditions in Fig. 2, the theoretical open-circuit voltage (zero current) is 1.169 V; note that measured open-circuit voltages are lower than theoretical ones owing to imperfect separation of the gases by the membrane and its finite electronic resistance. Increases in load current cause the cell voltage to decrease logarithmically owing to kinetic losses (green line in Fig. 2), with the large cell-voltage loss of about 370 mV in going from open-circuit voltage to practical currents of just 0.1 A cm^{-2} reflecting the sluggish ORR kinetics on Pt. The measured cell resistance multiplied by current density gives the iR losses, which can be added to the measured polarization curve (blue symbols) to give the iR-free curve (red symbols). The remaining difference between the iR-free curve and the ideal kinetic line represents the sum of all mass transport losses. In the range of practical current densities, 0.1–2.5 A cm^{-2}, improvements in MEA resistance can have a much larger impact on actual cell voltage than improvements in kinetics. Cell resistances have therefore been researched, and have been reduced nearly as much as is possible using current membranes and gas diffusion media. Kinetic losses are more challenging because an order-of-magnitude improvement in ORR activity would gain only 60–70 mV, and progress in catalyst development so far has achieved only modest cell voltage gains of tens of millivolts. Reducing mass transport overpotentials by the same amount is less difficult.

Targeted catalyst development benefits from a detailed understanding of the metal-catalysed electrochemical reduction of oxygen to water, $O_2 + 4H^+ + 4e^- \rightarrow 2H_2O$, which is mechanistically complicated. It is usually thought to involve different reaction pathways such as direct $4e^-$ reduction of adsorbed oxygen to water; or a $2e^-$ reduction to adsorbed H_2O_2 that then either desorbs or undergoes a second $2e^-$ reduction to water[11]. Irrespective of mechanistic detail, the kinetic current density i, normalized by the surface area of the Pt electrode and generated at a potential E, has been proposed[12] to be a function of the Gibbs energy of adsorption ΔG_{ad}

$$i = nFKc_{O_2}(1 - \Theta_{ad})^x \exp\left(-\frac{\beta FE}{RT}\right) \exp\left(-\frac{\gamma \Delta G_{ad}}{RT}\right) \quad (1)$$

where n, F, K, x, β, γ and R are constants, c_{O_2} is the molecular oxygen concentration, and Θ_{ad} the fraction of electrode surface sites covered with adsorbates. A key assumption in the development of the $(1 - \Theta_{ad})$ pre-exponential factor is that the ORR rate-limiting step is the first electron transfer step, $Pt(O_2)_{ad} + e^- \rightarrow Pt(O_2^-)_{ad}$, with

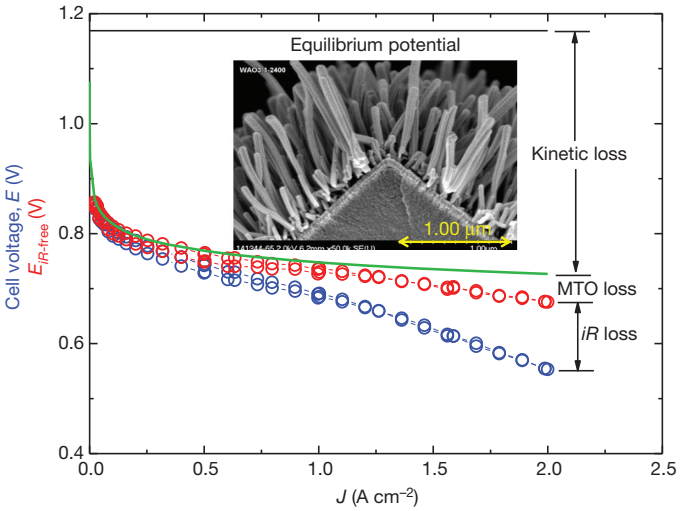

Figure 2 | Fuel-cell polarization curve. Measured PEM fuel-cell MEA polarization curve (blue) and iR-free (red) compared to a hypothetical curve for kinetic losses only (green). The difference gives the losses due to mass transport overpotentials (MTO). The polarization curve is from an MEA having electrodes based on the NSTF PtCoMn catalyst (inset) under 150 kPa H_2/air. Other conditions are given in ref. 23.

oxygen adsorption onto a surface primarily covered by impurities (hydroxyls) rather than reactive intermediates. This suggests that anything done to the surface's atomic or electronic structure that delays hydroxyls adsorbing and blocking O_2 adsorption sites will have a positive impact on the specific activity, because the $(1 - \Theta_{ad})$ term in equation (1) will be larger. This model underpins many approaches used to improve ORR electrocatalysts, although some recent model calculations and measurements are consistent with adsorbed oxygen or hydroxyl species playing a more active part as intermediates[6].

Electrocatalyst properties determining the observed current densities J (in A per planar cm^2) in MEAs are the electrode's electrochemically active surface area S (in cm^2 of Pt per planar cm^2), the kinetic current density i as in equation (1) that reflects the catalyst's activity, and a recently proposed[13] collision frequency scaling factor $f(\lambda, \rho_S)$ that depends on the mean free path length λ above the catalyst surface and on a spatial distribution function of surface area that to first order can be approximated by the catalyst surface area volumetric density ρ_S (in cm^2 Pt per cm^3). Or, in brief, $J = f \cdot S \cdot i$. The value of S is generally determined experimentally using cyclic voltammograms (see Box 1, which also provides catalyst activity definitions and DOE targets) and normalized by the electrode surface area to give the surface-area enhancement factor (in cm^2 of Pt per planar cm^2). Kinetic activity is measured *ex situ* in rotating disc electrode (RDE) apparatus[3,14,15] or *in situ* in fuel cells, with both methods requiring care to obtain reproducible results[3]. The two methods sample different surface states (that is, different amounts of hydroxyl or oxygen adsorption on platinum), so comparisons of RDE and fuel-cell activities are not always straightforward. The factor $f(\lambda,\rho_S)$, calculated from catalyst electrode physical properties, captures one way in which geometry has a differentiating role in comparing different electrocatalyst designs.

The basic electrocatalyst designs

PEM fuel-cell electrocatalyst technology has relied almost exclusively on either Pt blacks (metal particles so tiny that they absorb light very well and appear black, having a high surface to volume ratio, ideal for catalysts) or Pt nanoparticles, 2–5 nm in size, dispersed onto larger carbon black particles. Neither will meet the DOE 2017 performance and durability targets at PGM loadings that meet the cost targets. But our fundamental understanding of what controls catalytic activity has dramatically improved in the last few years and is now guiding next-generation catalyst development. Most emerging approaches focus on controlling the surface structure and composition of catalytic nanoparticles to achieve higher ORR activity with less Pt, and new synthetic routes have delivered such 'designer nanoparticles' that meet or exceed the DOE 2017 targets for ORR activity. However, the newest approaches are barely out of the 'test-tube' stage: they have not yet been tested extensively in actual fuel-cell MEAs, and it remains to be seen which approaches can also meet the other practical MEA requirements (see Table 1).

The basic designs for platinum catalysts are summarized in Fig. 3, categorized by overall geometry of the catalyst and its support and then further subdivided according to structural morphology and composition. This approach illustrates that kinetic activity can change by nearly an order of magnitude when the catalyst is a discrete nanoparticle or a polycrystalline thin film, and that catalyst surface area per unit volume can affect the maximum achievable current density. Also, the volume occupied by the non-active support influences current density[13], while aspect ratios determine the packing of the catalyst supports and hence porosity and free-radical scavenging.

BOX 1

Definitions and activity targets

- The surface-area enhancement factor is the Pt catalyst surface area S measured by the charge generated from an under-potential deposited monolayer of hydrogen atoms on the Pt catalyst surface divided by the planar area of the sample (cm^2 Pt per planar cm^2).
- Pt loading is the number of mg of Pt per planar cm^2 in an MEA electrode layer.
- Absolute ORR kinetic activity is currently defined as the current density measured at 900 mV under one atmosphere of fully saturated pure oxygen, at 80 °C. For an MEA this means 150 kPa absolute pressure, due to 50 kPa of water vapour.
- The area-specific activity A_s (A per cm^2 Pt) is determined by dividing the absolute activity by the surface-area enhancement factor.
- The mass activity A_m (A per mg of Pt) is determined by dividing the absolute activity by the Pt loading.
- The DOE's 2017 target for A_m is 0.44 A per mg Pt and its 2015 target for A_s is 0.7 mA per cm^2 Pt (ref. 1).

Extended surface area catalysts

Extended surface area (ESA) catalysts comprise large area surfaces extended in two dimensions like thin films. Their advantages over conventional Pt/C approaches are larger radii of curvature that make them more resistant to surface area loss via mechanisms such as Pt dissolution and redeposition, reduced mass transport losses, and in some cases the potential to eliminate corrosion of the catalyst support and simpler manufacturing. The area-specific ORR activities (A_s) of ESA catalysts are about ten times higher than nanoparticle-on-carbon catalysts, owing to electronic structure properties of thin films versus nanoparticles. Classic ESA examples are polycrystalline or single-crystalline bulk catalyst surfaces[16–20]; developed at Lawrence Berkeley and Argonne National Laboratory, these serve as valuable model systems that have shown the effect of structural aspects like single-crystal facet orientation, size, type and composition on activity. Some advanced ESA alloy catalysts exhibit a roughened 'Pt-skeleton' surface with Pt atoms covering the average bulk composition, or a highly coordinated pure 'Pt-skin' overlying a modulated surface structure in which the underlying three layers' composition oscillates towards the bulk composition[16,20]. Such a Pt-skin surface structure on Pt_3Ni_1 {111} was reported to have the world-record A_s of 18 mA per cm^2 Pt (non-*iR* corrected), about 90 times higher than a standard commercial dispersed Pt/C in comparative RDE measurements[16]. The peculiar arrangement of Pt and Ni atoms in the top three layers of this system causes different amounts of shift in the *d*-band centre relative to the Fermi level of the topmost layer of Pt atoms, which is believed to affect the adsorption coverage of hydroxyl spectator species that interfere with ORR (see equation (1)). The quest is how to achieve this in a practical catalyst.

Nanostructured thin-film (NSTF) catalysts are the only practical ESA catalysts found so far[13,21–24]. The support is a thin monolayer of an oriented array of crystalline organic whiskers, less than 1 μm tall and 30 nm × 55 nm in cross-section. It is applied to a roll-good substrate (a material made by a roll-to-roll process) with a number density of 30–40 whiskers per square micrometre, and then magnetron sputter-coated with catalyst thin films of choice (Fig. 2, inset). The organic support whisker is non-conductive, does not support corrosion currents and its body-centred cubic crystalline nature influences the subsequent nucleation and growth of the catalyst thin films coating them[25]. NSTF electrocatalysts have documented basic advantages in A_s of the catalyst[23,26], surface area utilization and stability[27,28], performance with ultralow PGM loadings[24], support corrosion resistance[29], high-volume manufacturability[30], and their release of F^- ions from the ionomer (perfluorosulphonic acid) used in the membrane or electrode is up to three orders of magnitude lower[24,31]. (Incomplete oxygen reduction to water on Pt produces H_2O_2, which creates free radicals that attack the membrane ionomer. Membrane degradation rates are proportional to the F^- ion release rates, with suppressed F^- release showing that the unique geometry of NSTF catalysts facilitates scavenging of radicals before they reach the membrane.) The low-volume support makes NSTF electrodes 10 to 20 times thinner than equivalently loaded Pt/C dispersed electrodes, which means better access to all of the catalyst surface area at all current densities. It also means less volume for

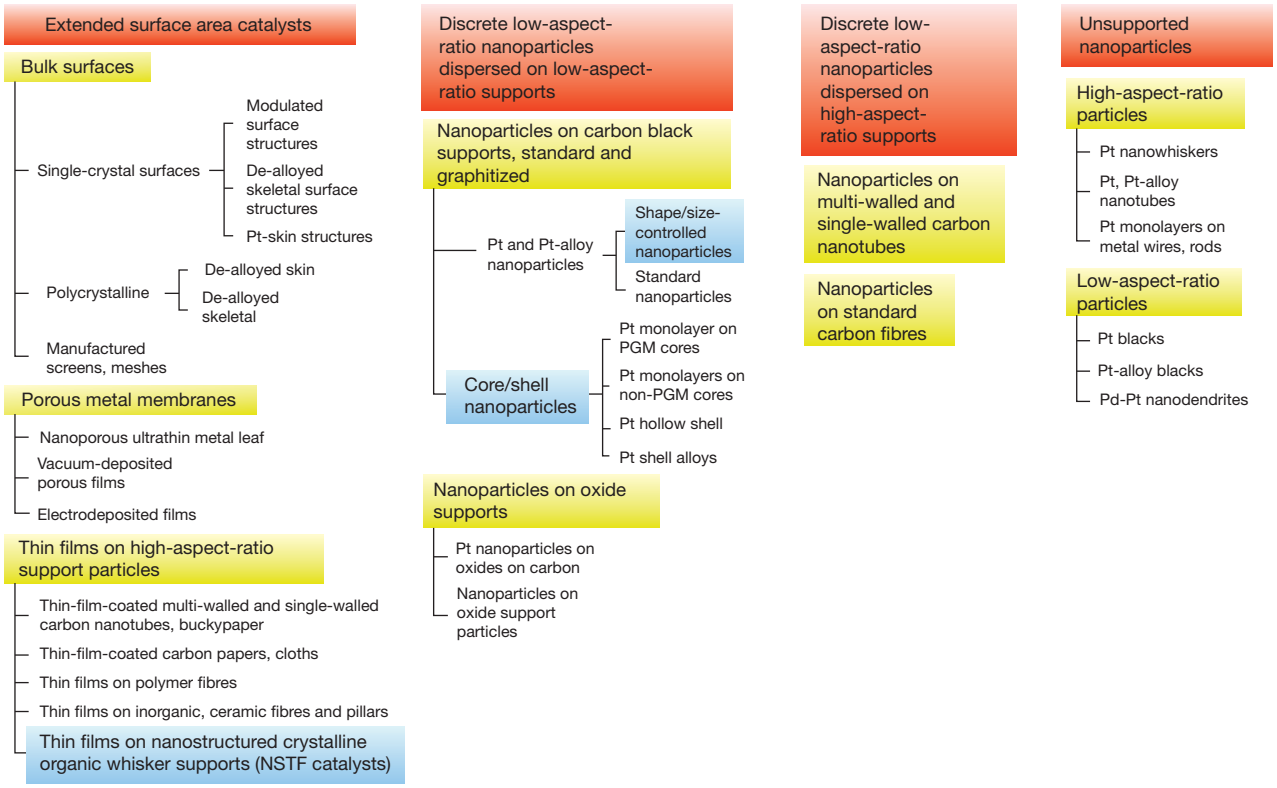

Figure 3 | Basic platinum-based heterogeneous electrocatalyst approaches. The four PEM fuel-cell electrocatalyst approaches (developed or under investigation) for the performance-limiting cathode ORR are shown, with Pt and Pt-alloy electrocatalysts listed according to the basic geometric structure of the catalyst particles and their supports. The main subcategories are highlighted in yellow. Catalyst approaches with the highest demonstrated activities are highlighted in blue.

storing any condensed product water that can lead to challenges in freeze-start, load transients (such as engine idling to full power as fast as possible) and cold operation, requiring different water-management strategies, anode gas diffusion layers, or modifications of operating protocols[32]. NSTF Pt alloys show the same activity gains over pure Pt as dispersed nanoparticles. De-alloying (see Box 2 for details) can endow the NSTF catalyst coating with core–shell properties as well, with sublayers affecting the lattice properties of the outermost Pt surface. The NSTF alloy catalyst with the largest production to date uses the $Pt_{68}Co_{29}Mn_3$ composition, which for loadings of 0.05–0.15 mg cm^{-2} delivers A_s values of 1.3–1.8 mA cm^{-2} Pt, and mass activities (A_m) of 0.15–0.17 A cm^{-2} Pt. Still under development are NSTF $Pt_{1-x}Ni_x$ alloy catalysts with an unusually sharply peaked gain in activity for $x = 0.7$ (ref. 33). They reach $A_s \approx 2.4$ mA cm^{-2} Pt and A_m from 0.24 to over 0.5 A mg^{-1} Pt in 50-cm^2 fuel-cell measurements, with loadings below 0.15 mg Pt cm^{-2} (refs 23, 24).

In related approaches, thin catalyst films are applied to single- or multi-wall carbon nanotubes[34,35] to achieve higher activity on a more durable support. These systems are more durable[35] than catalysts on high-surface-area carbons, but performances and activities have not improved significantly and the nanotubes will still ultimately corrode at high potentials.

Porous metal membranes[36–40], the third class of extended surface area catalysts, include nanoporous ultrathin metal leaves and vacuum-deposited, electrodeposited or laser-deposited porous films. They can be de-alloyed (see Box 2 for more details) to create nanoporosity, or to obtain specific modulated surface layer compositions similar to that of the Pt_3Ni_1 {111} system. These catalysts show high specific A_s values similar to those of polycrystalline bulk surfaces but with higher surface area, and enable valuable studies of the de-alloying processes, but are mostly not amenable to high-volume manufacturing.

Nanoparticles on low-aspect-ratio supports

This catalyst category is dominated by roughly spherical Pt or Pt alloy nanoparticles dispersed on standard or graphitized carbon black support particles, including conventional homogeneous Pt and Pt transition-metal alloy nanoparticles[3,19,41–43] and designer nanoparticles with size, shape and radial composition controlled to increase activity and reduce Pt.

BOX 2

De-alloying of Pt transition-metal alloys

The de-alloying of less-noble elements from Pt-alloys is a key strategy for creating Pt-based catalysts in all design categories. This means less stable elements initially alloyed with Pt (usually at a high atomic percentage of transition metal) are intentionally or unintentionally dissolved out to leave a nanoporous film, or skeletal surface or core–shell particle configuration[37,38,88] overlying a composition closer to a stable bulk alloy composition such as Pt_3M_1, where M is a transition metal. The process increases surface area, and creates in the outer few layers a modulated surface composition that leaves the surface Pt lattice contracted or its electronic structure favourably modified, as illustrated by lattice-strain control of the Pt shells formed around de-alloyed cores[94]. In the case of $Pt_{1-x}Ni_x$ bulk alloys with high Ni content, electrochemical de-alloying provide a means of studying[95–97] the evolution of nanoporosity. The resultant material, with average pore and ligament sizes of 3–5 nm and filled with hydrophobic protic liquids, displayed $S_m = 44$ m^2 per g Pt, and $A_m = 0.4$ A per mg Pt[95]. Strasser and colleagues have pioneered voltammetric de-alloying of electrode nanoparticles, composed of base-metal-rich bimetallic and trimetallic alloys[88,91,92,94], directly in the MEA and reported A_s and A_m values exceed the DOE 2017 and 2015 targets (Box 1). Although such *in situ* methods are not practical, understanding the de-alloying process is critical for optimizing the catalyst properties and *ex situ* de-alloying of these alloy systems is under investigation[93].

The state-of-the-art of conventional Pt and Pt-alloy/C electrocatalysts in dominant use today consist of Pt nanoparticles with diameters of 2–4 nm, dispersed onto larger high-surface-area carbon black support particles at Pt/C weight percentages of 20% to 60%. Commercial pure Pt/C catalysts have surface areas of 80–120 $m^2 g^{-1}$ Pt, specific activities of 0.15–0.2 mA cm^{-2} Pt and mass activities of 0.1 to 0.12 A mg^{-1} Pt measured in MEAs. Homogeneous Pt-alloy nanoparticles on carbon have historically been observed to increase ORR activity over pure Pt/C by about a factor of 2 to 2.5. The commercially available, heat-treated 30 weight per cent PtCo/C system routinely provides MEA measurement values of specific and mass activity in our 3M laboratory that are close to the DOE targets, for example, 1.2 mA cm^{-2} Pt and 0.39 A mg^{-1} Pt. For a wide range of carbon-based supports, initial Pt surface areas range from 20 to over 70 $m^2 g^{-1}$ Pt, but converge after stability testing to 20–30 $m^2 g^{-1}$ Pt (ref. 44).

Uniformly sized octahedra, cubes or other polyfaceted shapes identically terminated with {111} and {100} facets[45–48]can be produced, often using capping agents selectively to control facet growth rates. Truncated-octahedral Pt_3Ni particles with predominantly {111} facets show A_m values up to four times those of commercial Pt/C (ref. 46), and much higher than {100} bounded cubes[47]. Surface-specific activity strongly depends on the fraction of {111} surface exposed and is about a tenth that of bulk single-crystal Pt_3Ni{111} surfaces, suggesting that larger shape-controlled particles with higher surface coordination (fewer surface defects where oxides preferentially form) or compositional gradients could improve activities[49]. In the case of monodispersed Pt_3Co nanoparticles, these factors increase grain size and A_s monotonically for particle sizes of 3–9 nm, while A_m peaks at about 4.5 nm for optimum particle annealing at 500 °C (refs 45, 50). Monodispersed and homogeneous $Pt_{1-x}Ni_x$ nanoparticles with controlled Ni depletion from the outer surface layers exhibit a Pt-skeleton-type surface structure, with the improvement factor over Pt/C peaking at 4.5 nm for monodispersed PtNi (ref. 51). For similarly structured PtCoNi alloy particles, mass activities by RDE are reported to exceed 2.5 A mg^{-1} Pt (ref. 52).

Core–shell nanoparticle electrocatalysts pioneered at Brookhaven National Laboratory constitute a highly promising subcategory of catalysts[52–64]. These systems exhibit higher mass activities because Pt is eliminated from the core of the catalyst particles, and higher specific activities because the core material influences the outer Pt monolayer and optimizes its surface electronic and structural properties. Examples include Pt monolayers on Pd and non-PGM cores, de-alloyed cores, 'Swiss-Pt' de-alloyed cores (full of pores), and hollow Pt or Pt-alloy shells[53,54,57–63]. The core material would ideally consist of non-PGM elements, though the successful Pt-monolayer core–shell catalysts so far have cores containing Pd, Au-Ni, Pd-Co, Pd_3Co, Pd_3Fe, Pd-Ir, Ir, Pd-Au, $AuNi_{0.5}Fe$, Pd-Nb, Pd-V, Pd-W and Ru monolayers on Pd cores. Fuel-cell MEA measurements with these novel catalysts at two industrial locations yield mass activities lower than the RDE values measured by the Brookhaven National Laboratory group[59,64], which may be due to non-optimized electrodes. Key development opportunities for this subcategory include development of scalable synthetic routes for generating 'pin-hole'-free Pt monolayers to protect the non-PGM core material from leaching; increasing specific activity while using less expensive core materials and optimizing electrode ink formulations; and further increased resistance to Pt dissolution due to repeated start-stop induced voltage cycling events.

Support corrosion is a problem for all these systems, pushing development towards dispersing the nanoparticle catalysts on graphitized, lower-surface-area carbons or single-wall or multi-wall carbon nanotubes (see below). Another strategy uses inherently more stable inorganic oxides as support. If these provide adequate conductivity, for example, where the oxide support is formed on carbon black, promising mass activities are obtained: 0.2 A mg^{-1} Pt for Pt/C, 0.3 A mg^{-1} Pt for Pt-$TaOPO_4$/C and 0.45 A mg^{-1} Pt for heat-treated Pt-$TaOPO_4$/C (where C = Vulcan carbon)[65].

Nanoparticles on high-aspect-ratio supports

This category includes Pt or Pt-alloy nanoparticles dispersed on standard carbon fibres as well as on single- or multi-walled carbon nanotubes[66]. As in the case of thin-film catalysts coated onto these types of supports, the objective is usually improved durability because the activity of the nanoparticles is not expected to change much with the aspect ratio of the support. In the case of carbon nanotube supports, their higher electrical conductivity is not really any advantage because electronic impedance of the electrodes is a very small contributor to the overall overpotential losses, but carbon nanotube supports can improve transport or water management[67]. However, concerns about the possible adverse health effects of carbon nanotubes without the counterweight of a significant functional performance or processing advantage may make them unattractive for high-volume electrode manufacturing.

Unsupported nanoparticles

Unsupported nanoparticle catalysts include the traditional low-aspect-ratio particles of Pt and Pt alloy blacks[41], and new concepts that use Pt and Pt-alloys in the form of high-aspect-ratio structures such as nanotubes[68,69]and Pt monolayers on Pd nanowires and nanorods[70,71]. Although they are just at the initial-concept phase, the unsupported metal nanotube catalysts are claimed to improve A_s values over bulk polycrystalline Pt by a factor of eight (ref. 69), and the monolayer systems are claimed to exhibit impressive mass activities of 0.4 A mg^{-1} PGM[70,71](measured by RDE).

Pt-free electrocatalysts

Owing to the scarcity and high cost of Pt, Pd-based catalysts (recently reviewed by Shao[72]) and Pd-based transition metal alloy catalysts (explored in the Myers group[73]) have been considered. But the best activities reported for Pd are barely equivalent to typical Pt/C, with the best use of Pd appearing to be in combination with Pt as in the core–shell configurations discussed above. In any case, replacement of most of the Pt by Pd may not significantly address the cost issue, owing to demand/price fluctuations[2].

Non-precious metal (NPM) catalysts eliminate PGMs completely to reduce costs, and have recently shown dramatic ORR activity improvements. Among the many approaches being explored[74–83], pyrolysis of cobalt- and iron-containing heteroatom polymer precursors (for example, porphyrins) has been the dominant route towards NPM catalysts. Active sites are believed to comprise metals coordinated to several nitrogen atoms, MN_x (where M = Co, Fe). The Dodelet group's impregnation and pyrolysis process combining Fe precursors and a nitrogen precursor has led to the largest beginning-of-life activity increases[79,81]. The nature of the active site in these NPM catalysts is still debated, as is the question of whether Fe is associated with the active site or with the means of creating such a site. There is no way to measure area density of active sites as for Pt-based catalysts, so kinetic activity is reported as a volumetric current density. Kinetic activities measured at 0.8 V using pure O_2 have rapidly increased from 2.7 A cm^{-3} in 2008 (ref. 82), to 99 A cm^{-3} in 2009 (ref. 79), and 230 A cm^{-3} in 2011 (ref. 81). The most recent increase was due to a large reduction in mass transport loss: the performance of a new NPM Fe-based cathode on Nafion 117 ionomer under 2-bar gauge H_2/air was 0.25 A cm^{-2} at 0.5 V after 100 hours, about a tenth of the current density obtained with Pt-based cathodes. The key issues for NPM catalysts are mass transport losses and stability. A polyaniline FeCo-C catalyst with relatively high durability (700 hours) at 0.4 V in a H_2/air fuel cell and a peak power density of 0.55 W cm^{-2} at 0.38 V under pressurized pure oxygen has been reported[83]. But NPM catalyst durability is worse at higher potentials—and for automotive purposes, performances at less than 0.6 V are largely irrelevant.

Comparison of kinetic activities

As illustrated by the preceding discussion, a wide range of catalyst systems has been explored and Fig. 4 shows composite plots of A_m versus

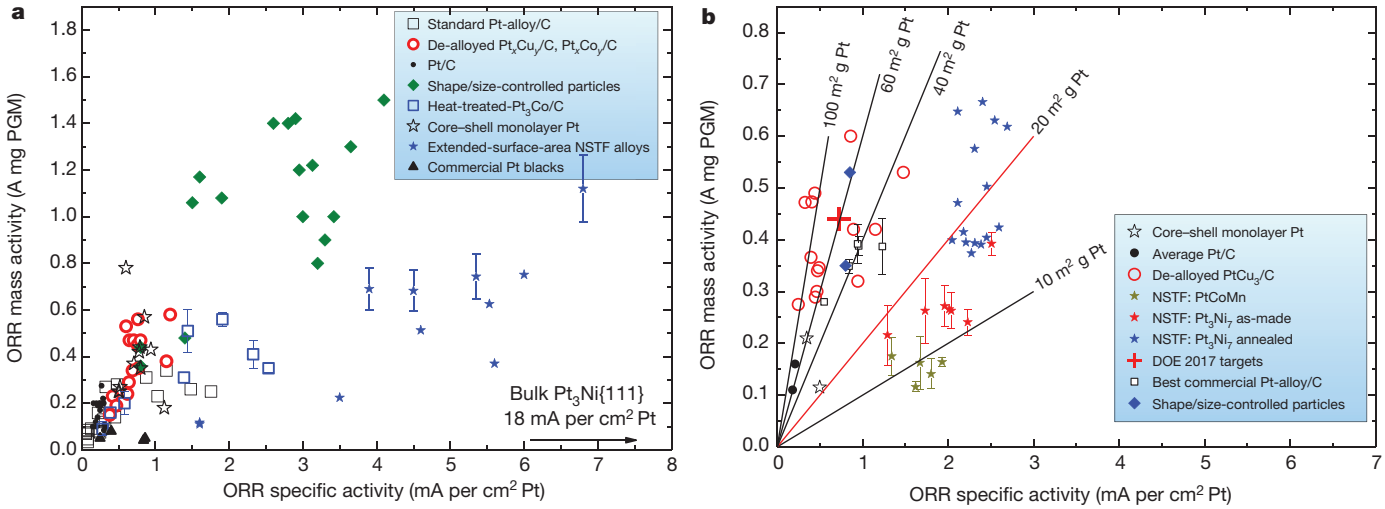

Figure 4 | Kinetic activities of the main Pt-based electrocatalyst systems. The ORR A_m versus A_s are shown for the major Pt-based electrocatalyst approaches listed in Fig. 3. **a**, Activities are measured by RDE at 900 mV for the following catalysts: standard Pt-alloys/C (refs 42, 43, 87), de-alloyed PtM_3/C (where M = Cu, Co) (refs 88–90), Pt/C (refs 3, 42, 44, 46–48, 50), shape- and size-controlled particles (refs 45, 47, 48, 50, 51), heat-treated Pt_3Co/C (ref. 42), core–shell monolayer Pt (refs 44, 56, 60, 62–64, 71), extended-surface-area NSTF alloys (refs 23,26) and commercial Pt blacks (refs 3, 48). **b**, Activities are measured in MEAs at 900 mV, 80 °C and 150 kPa saturated O_2 for the following catalysts: core–shell Pt monolayer (refs 49, 64), average Pt/C (refs 3, 91, 92), de-alloyed $PtCu_3$/C (refs 91–93), three extended-surface-area NSTF alloys (ref. 23), the DOE 2017 and 2015 targets, best commercial Pt-alloys/C (data from GM, 3M), and shape- and size-controlled particles (refs 46, 52). The scattering of activity values for any one type or reference represent different catalyst compositions, loadings or preparation and process treatments, not statistical variations in measurement.

A_s measured by both RDE and in MEAs for the most promising ones. RDE values are generally larger than those measured in MEAs, reflecting not only the more complex environment of the catalyst in a working fuel cell but also the simple difference in protocol that allows RDE measurements on a clean surface while MEA values are obtained with oxidized surfaces. (Note that RDE measurements will also depend on temperature, voltage scan rate, *iR* and diffusion-correction factors.) For standard Pt/C or Pt alloy/C catalysts, only a few data points are given to represent generally accepted measured values. The figures show that several catalyst systems seem to be able to meet the DOE 2017 A_m target of 0.44 A mg^{-1} Pt; some systems come very close, including the best commercial Pt-alloy/C catalyst, for which durability is still an issue. The highest-performing systems in Fig. 4 are not yet practical, in that they are not able to simultaneously satisfy all the electrocatalyst requirements for high current density and durability at low loadings.

Manufacturing and scalability

Manufacturability and quality control of MEAs produced at the rates ultimately required for true commercialization have not been an issue for the small fuel-cell vehicle fleets produced to date. But the lead time to get an MEA component qualified for insertion into a vehicle stack is about five years, and publicly announced future emergent fuel-cell vehicle volumes are tens to hundreds of thousands of vehicles per year by 2020. Clearly, the scalability of any new catalyst approach now has to be seriously considered from the outset. For many of the new catalyst approaches being evaluated at the 'test-tube' stage, it is not clear that the processes used to generate them would be scalable with the quality levels required. The DOE cost targets are based on 500,000 vehicles per year, and a particular MEA technology advanced to that emergent market level will not be easily discarded in favour of something totally new that may be better able to reach a more mature production level at say 10% of the world market in 2030 (or 15 million vehicles).

To illustrate the scales involved, consider that annual production of 15 million fuel-cell vehicles each with a stack containing 300 (versus the 400 required today) MEAs (each around 300 cm^2) would require 4.50 billion MEAs a year. With a production line at full capacity operating three shifts per day, 360 days per year, or about 8,000 hours per year with 80% average up-time to account for maintenance, repair and lot changes of input materials, the required production rate is about 11,700 MEAs per minute. To match car production at about one vehicle per minute per production line, or 300 MEAs per stack per minute, would require 20 full-capacity MEA production lines each producing 585 MEAs per minute or about 10 MEAs per second (with more production lines requiring more capital and operating costs). Individual piece part processing is out of the question.

Target loadings of about 0.1 mg Pt per cm^2 mean electrode thicknesses will be less than 2 μm, requiring precision coating methods with critical limits on debris and tolerances. High-volume roll-to-roll widths up to a metre in width should be possible, so even with ten MEAs across the web width, each measuring 10 cm × 30 cm, line speeds of 20 m min^{-1} will be required. These MEAs have to be made with extraordinary quality control (one fatal MEA defect in 30,000 MEAs for 1% stack failures). The catalyst and catalyst/membrane integration manufacturing processes have to be simple, robust, few in number and have wide process parameter windows, given that the yields per step multiply. Just four sequential process steps with 90% yields would increase costs by 30% without recycling. Process steps for electrode formation that require hot bonding, annealing, solvent evaporation or drying steps lasting for minutes will require proportionately long manufacturing lines. Build-up of residues on the coaters, 8-hour shift lengths, ability to handle jumbo roll-goods, safety and catalyst batch-size limitations will be factors affecting batch sizes, throughputs and labour costs. At loading targets of even 0.125 mg cm^{-2} on MEAs with 300 cm^2 active areas, the above line speeds require catalyst flow-through rates of 1.5 kg of Pt per hour—roughly US$2 million worth of Pt per day per manufacturing line, at a metal price of US$2,000 troy ounces. On-site recycling of scrap will probably be justified. Recycling of Pt, once it reaches the target stack loadings equivalent to the PGM amounts used in current internal combustion engines, will be justified by the same economic arguments currently used for recycling PGMs in catalytic converters. Ink mixing of dispersions for catalyst coating, if used, would have to keep pace and use chemistries compatible with coating line speeds and quality levels. Safety, environmental and cost control requirements will probably exclude coating processes using flammable solvents. I believe these requirements and the required production rates and levels of quality will ultimately result in catalyst layer coating by all-dry vacuum-coating methods, such as the method used to produce over 80% of the world's multi-layer optical-film-coated glass that is used in low-emissivity windows and produced at a

volume of 250 million square metres already in 2005 (ref. 84). All the above considerations regarding essential process requirements apply to catalyst-membrane integration and the fabrication and integration of other stack components as well.

Perspective

Several catalyst systems have ORR kinetics adequate for automotive applications, including commercially available heat-treated PtCo/C. But at the required low PGM loadings, none are able yet to deliver in a fuel-cell environment the necessary high power, durability or robustness. Recent progress with 'designer' catalyst particles and ESA catalysts suggests that they will reach over the next few years their maximum kinetic performance, something close to the specific activity of 18 mA per cm^2 Pt measured by RDE on bulk crystals of $Pt_3Ni\{111\}$. The consistent difference between RDE and MEA values (see Fig. 4) implies that this ultimate performance maximum will be about 6–9 mA per square centimetre of Pt in a fuel-cell environment, well above the DOE 2017 target. But as the discussion of additional practical requirements and manufacturing issues has shown, impressive kinetic activity will not suffice to make a catalyst system attractive for large-scale automotive MEA production. I therefore consider that realizing target ORR activities may no longer be the most important goal, despite being the overwhelming focus of many researchers in the field. Instead, we should aim to achieve (at the required low PGM loadings) the durability and power targets using something that can be manufactured at high volumes with the requisite quality, throughput and yields. This poses a considerable challenge to the community, particularly when considering that for most catalyst systems durability, high power performance, quality and yield decrease as loadings decrease.

Grounds for optimism are the recent pace and diversity in the development of interesting new approaches to PEM fuel-cell electrocatalysts that optimize ORR kinetic activities without sacrificing durability or cost. A few material and design concepts are guiding these efforts, namely the use of extended-surface-area catalyst geometries; the use of alloys, particularly with Ni; the synthesis of catalysts with large, highly coordinated {111} facets; and the use of de-alloyed or annealed surface structures with increased surface area and a modulated composition that improves the activity of the topmost Pt layer. The ideal catalyst would embody all of these improvement characteristics[22].

These recent developments illustrate that the level and quality of fundamental research in the field need to continue unabated. Particularly beneficial would be a clear understanding of surface area and activity loss mechanisms, and insight into the causes of durability loss[85,86] associated with externally and internally generated impurities. I also hope for future electrocatalyst research exploring how membrane and microporous materials in contact with the catalyst and off-nominal operating events affect performance. We also need to know whether there are any fundamental processing rate limitations on high-volume manufacturability. These are the issues that will arise when the rubber meets the road, and will dictate the ultimate costs and customer acceptance of fuel-cell vehicles. It has been eighteen years since the first PtCo/C catalyst was investigated, but it is still not generally accepted for use in current fuel-cell vehicles; it may take even longer to implement any of the newer catalyst approaches into realistic electrodes.

1. The. US Department of Energy (DOE). *Energy Efficiency and Renewable Energy* http://www.eere.energy.gov/hydrogenandfuelcells/mypp/pdfs/fuel_cells.pdf and the *US DRIVE Fuel Cell Technical Team Technology Roadmap* (revised 25 January 2012) www.uscar.org/guest/teams/17/Fuel-Cell-Tech-Team.
These websites define the most critical performance, durability and cost targets for the PEM fuel-cell MEA and each of its components, as well as stack and system requirements.
2. Wagner, F. T., Lakshmanan, B. & Mathias, M. F. Electrochemistry and the future of the automobile. *J. Phys. Chem. Lett.* **1,** 2204–2219 (2010).
3. Gasteiger, H., Kocha, S., Sompalli, B. & Wagner, F. Activity benchmarks and requirements for Pt, Pt-alloy, and non-Pt oxygen reduction catalysts for PEMFCs. *Appl. Catal. B* **56,** 9–35 (2005).
This paper first defined and explained the ORR activity targets and requirements for the PEM fuel-cell cathodes, particularly for fuel-cell vehicles.
4. Markovic, N., Schmidt, T., Stamenkovic, V. & Ross, P. Oxygen reduction reaction on Pt and Pt bimetallic surfaces: a selective review. *Fuel Cells* **1,** 105–116 (2001).
5. Nørskov, J. K., Bligaard, T., Rossmeisl, J. & Christensen, C. H. Towards the computational design of solid catalysts. *Nature Chem.* **1,** 37–46 (2009).
6. Greeley, J. *et al.* Alloys of platinum and early transition metals as oxygen reduction electrocatalysts. *Nature Chem.* **1,** 552–556 (2009).
7. Wipke, K, *et al. Controlled Hydrogen Fleet and Infrastructure Analysis: 2011 DOE Hydrogen Program Annual Merit Review and Peer Evaluation Meeting* http://www.hydrogen.energy.gov/pdfs/review11/tv001_wipke_2011_o.pdf (National Renewable Energy Laboratory, 2011).
8. Reiser, C. A. *et al.* A reverse-current decay mechanism for fuel cells. *Electrochem. Solid-State Lett.* **8,** A273 (2005).
This explains the basic mechanism by which fuel starvation or start-up and shut-down events in a PEM fuel cell can cause carbon corrosion on the cathode.
9. Atanasoska, L. L., Vernstrom, G. D., Haugen, G. M. & Atanasoski, R. T. Catalyst durability for fuel cells under start-up and shutdown conditions: evaluation of Ru and Ir sputter-deposited films on platinum in PEM environment. *ECS Trans.* **41,** 785–795 (2011).
10. Halalay, I. C. *et al.* Anode materials for mitigating hydrogen starvation effects in PEM fuel cells. *J. Electrochem. Soc.* **158,** B313–B321 (2011).
11. Sepa, D. B., Vojnovic, M. V. & Damjanovic, A. Reaction intermediates as a controlling factor in the kinetics and mechanism of oxygen reduction at platinum electrodes. *Electrochim. Acta* **26,** 781–793 (1981).
12. Markovic, N. M. & Ross, P. N. Surface science studies of model fuel cell electrocatalysts. *Surf. Sci. Rep.* **45,** 117–229 (2002).
13. Debe, M. K. Effect of electrode surface area distribution on high current density performance of PEM fuel cells. *J. Electrochem. Soc.* **159,** B54–B67 (2012).
14. Mayrhofer, K. J. J. *et al.* Measurement of oxygen reduction activities via the rotating disc electrode method: from Pt model surfaces to carbon-supported high surface area catalysts. *Electrochim. Acta* **53,** 3181–3188 (2008).
15. Garsany, Y., Barurina, O. A., Swider-Lyons, K. E. & Kocha, S. S. Experimental methods for quantifying the activity of platinum electrocatalysts for the oxygen reduction reaction. *Anal. Chem.* **82,** 6321–6328 (2010).
16. Stamenkovic, V. R. *et al.* Improved oxygen reduction activity on $Pt_3Ni(111)$ via increased surface site availability. *Science* **315,** 493–497 (2007).
This paper showed that the fundamental kinetic activity for oxygen reduction on bulk Pt–Ni alloy surfaces could be nearly two orders of magnitude higher than the standard dispersed Pt on carbon.
17. Stamenkovic, V. R., Mun, B. S., Mayrhofer, K. J. J., Ross, P. N. & Markovic, N. M. Effect of surface composition on electronic structure, stability and electrocatalytic properties of Pt-transition metal alloys: Pt-skin versus Pt-skeleton surfaces. *J. Am. Chem. Soc.* **128,** 8813–8819 (2006).
This paper demonstrates the sensitivity and specificity of ORR activity to the fundamental surface structure and composition of the top few layers of Pt transition metal alloys.
18. Stamenkovic, V. R. *et al.* Trends in electrocatalysis on extended and nanoscale Pt-bimetallic alloy surfaces. *Nature Mater.* **6,** 241–247 (2007).
19. Paulus, U. A. *et al.* Oxygen reduction on high surface area Pt-based alloy catalysts in comparison to well defined smooth bulk alloy electrodes. *Electrochim. Acta* **47,** 3787–3798 (2002).
20. Stamenković, V., Schmidt, T. J., Ross, P. N. & Markovic, N. M. Surface composition effects in electrocatalysis: kinetics of oxygen reduction on well-defined Pt_3Ni and Pt_3Co alloy surfaces. *J. Phys. Chem. B* **106,** 11970–11979 (2002).
21. Debe, M. K. in *Handbook of Fuel Cells—Fundamentals, Technology and Applications* (eds Vielstich, W., Lamm, A. & Gasteiger, H. A.) Ch. 45 (John Wiley & Sons, 2003).
22. Debe, M. K., Atanasoski, R. T. & Steinbach, A. J. Nanostructured thin film electrocatalysts—current status and future potential. *ECS Trans.* **41,** 937–954 (2011).
23. Debe, M. K. *2009–2011 Annual Merit Reviews DOE Hydrogen and Fuel Cells and Vehicle Technologies Programs: Advanced Cathode Catalysts and Supports for PEM Fuel Cells* http://www.hydrogen.energy.gov/pdfs/review11/fc001_debe_2011_o.pdf (DOE, 2011).
24. Debe, M. K. Nanostructured thin film electrocatalysts for PEM fuel cells—a tutorial on the fundamental characteristics and practical properties of NSTF catalysts. *ECS Trans.* **45** (2), 47–68 (2012).
This paper defines all the catalyst and MEA measured properties and published papers so far for the NSTF type catalyst electrodes.
25. Gancs, L., Kobayashi, T., Debe, M. K., Atanasoski, R. & Wieckowski, A. Crystallographic characteristics of nanostructured thin film fuel cell electrocatalysts—a HRTEM study. *Chem. Mater.* **20,** 2444–2454 (2008).
26. van. der Vliet, D. *et al.* Platinum-alloy nanostructured thin film catalysts for the oxygen reduction reaction. *Electrochim. Acta* **56,** 8695–8699 (2011).
27. Debe, M. K., Schmoeckel, A. K., Vernstrom, G. D. & Atanasoski, R. High voltage stability of nanostructured thin film catalysts for PEM fuel cells. *J. Power Sources* **161,** 1002–1011 (2006).
28. Debe, M. K., Steinbach, A. J. & Noda, K. Stop-start and high-current durability testing of nanostructured thin film catalysts for PEM fuel cells. *ECS Trans.* **3,** 835–853 (2006).
29. Debe, M. K. *et al.* Durability aspects of nanostructured thin film catalysts for PEM fuel cells. *ECS Trans.* **1,** 51–56 (2006).
30. Debe, M. K. *et al.* in *Proc. 50th Annual Technical Conference of the Society of Vacuum Coaters* 175–185 (The Society of Vacuum Coaters, 2006).
31. Haugen, G., Barta, S., Emery, M., Hamrock, S. & Yandrasits, M. in *Fuel Cell Chemistry and Operation* (eds Herring, A. M., Zawodzinski Jr., T. A. & Hamrock, S. J.) 137 (ACS Symposium Series 1040, 2010).
32. Steinbach, A. *et al.* Influence of anode GDL on PEMFC ultra-thin electrode water management at low temperatures. *ECS Trans.* **41,** 449–457 (2011).

33. Debe, M. K. *et al.* Extraordinary oxygen reduction activity of Pt_3Ni. *J. Electrochem. Soc.* **158,** B910–B918 (2011).
34. Park, S. *et al.* Polarization losses under accelerated stress test using multiwalled carbon nanotube supported Pt catalyst in PEM fuel cells. *J. Electrochem. Soc.* **158,** B297–B302 (2011).
35. Wang, S., Jiang, S. P., White, T. J. & Wang, X. Synthesis of Pt and Pd nanosheaths on multi-walled carbon nanotubes as potential electrocatalysts of low temperature fuel cells. *Electrochim. Acta* **55,** 7652–7658 (2010).
36. Yang, R., Leisch, J., Strasser, P. & Toney, M. F. Structure of dealloyed $PtCu_3$ thin films and catalyst activity for oxygen reduction. *Chem. Mater.* **22,** 4712–4720 (2010).
37. Erlebacher, J. & Snyder, J. Dealloyed nanoporous metals for PEM fuel cell catalysis. *ECS Trans.* **25,** 603–612 (2009).
38. Erlebacher, J., Aziz, M., Karma, A., Dimitrov, N. & Sieradzki, K. Evolution of nanoporosity in dealloying. *Nature* **410,** 450–453 (2001).
39. Moffat, T. P., Mallett, J. J. & Hwang, S.-M. Oxygen reduction kinetics on electrodeposited $Pt_{100-x}Ni_x$, and $Pt_{100-x}Co_x$. *J. Electrochem. Soc.* **156,** B238–B251 (2009).
40. Imbeault, R., Antonio, P., Garbarino, S. & Guay, D. Oxygen reduction kinetics on Pt_xNi_{100-x} thin films prepared by pulsed laser deposition. *J. Electrochem. Soc.* **157,** B1051–B1058 (2010).
41. Ralph, T. R. & Hogarth, M. P. Catalysis for low temperature fuel cells. *Platin. Met. Rev.* **46,** 3–14 (2002).
42. Schulenburg, H. *et al.* Heat-treated PtCo nanoparticles as oxygen reduction catalysts. *J. Phys. Chem. C* **113,** 4069–4077 (2009).
43. Thompsett, D. in *Handbook of Fuel Cells—Fundamentals, Technology and Applications* (eds Vielstich, W., Lamm, A. & Gasteiger, H. A.) Ch. 37 (John Wiley & Sons, 2003).
44. Wagner, F. T. Automotive Challenges and Opportunities for Oxygen Reduction Catalysts. In *First CARISMA Intl Conf.* (La Grande Motte, France, 23 September 2008).
45. Wang, C. *et al.* Monodisperse Pt_3Co nanoparticles as electrocatalyst: the effects of particle size and pretreatment on electrocatalytic reduction of oxygen. *Phys. Chem. Chem. Phys.* **12,** 6933–6939 (2010).
46. Wu, J. B. *et al.* Truncated octahedral Pt_3Ni ORR electrocatalysts. *J. Am. Chem. Soc.* **132,** 4984–4985 (2010).
47. Zhang, J., Yang, H., Fang, J. & Zou, S. Synthesis and oxygen reduction activity of shape-controlled Pt_3Ni nanopolyhedra. *Nano Lett.* **10,** 638–644 (2010).
48. Lim, B. *et al.* Pd-Pt bimetallic nanodendrites with high activity for oxygen reduction. *Science* **324,** 1302–1305 (2009).
49. Gasteiger, H. A. & Markovic, N. M. Just a dream—or future reality? *Science* **324,** 48–49 (2009).
50. Wang, C. *et al.* Monodisperse Pt_3Co nanoparticles as a catalyst for the oxygen reduction reaction: size-dependent activity. *J. Phys. Chem. C* **113,** 19365–19368 (2009).
51. Wang, C. *et al.* Correlation between surface chemistry and electrocatalytic properties of monodispersed Pt_xNi_{1-x} nanoparticles. *Adv. Funct. Mater.* **21,** 147–152 (2011).
52. Markovic, N. Nanosegregated cathode catalysts with ultra-low platinum loading. In *2010 DOE Hydrogen Program Annual Merit Review* FC-006, http://www.hydrogen.energy.gov/pdfs/review10/fc008_markovic_2010_o_web.pdf (2011).
53. Shao, M., Sasaki, K., Marinkivic, N. S., Zhang, L. & Adzic, R. R. Synthesis and characterization of platinum monolayer oxygen-reduction electrocatalysts with Co-Pd core-shell nanoparticle supports. *Electrochem. Commun.* **9,** 2848–2853 (2007).
54. Bliznakov, S. T., Vukmirovic, M. B., Yang, L., Sutter, E. A. & Adzic, R. R. Pt monolayer on electrodeposited Pd nanostructures—advanced cathode catalysts for PEM fuel cells. *ECS Trans.* **41,** 1055 (2011).
55. Vukmirovic, M. B. *et al.* Platinum monolayer electrocatalysts for oxygen reduction. *Electrochim. Acta* **52,** 2257–2263 (2007).
56. Shao, M. H., Sasaki, K., Lui, P. & Adzic, R. R. Pd_3Fe and Pt monolayer Pd_3Fe electrocatalysts for oxygen reduction. *Z. Phys. Chem.* **221,** 1175–1190 (2007).
57. Zhang, J. *et al.* Platinum monolayer electrocatalysts for O_2 reduction: Pt monolayer on Pd(111) and on carbon-supported Pd nanoparticles. *J. Phys. Chem. B* **108,** 10955–10964 (2004).
58. Russell, A. E. *et al.* In situ XAS studies of core-shell PEM fuel cell catalysts: the opportunities and challenges. *ECS Trans.* **41,** 55–67 (2011).
59. Haug, A. *et al.* Stability of a Pt-Pd core-shell catalyst: a comparative fuel cell and RDE study. *218th ECS Meeting* abstr. 743 (The Electrochemical Society, 2010).
60. Knupp, S. L. *et al.* Platinum monolayer electrocatalysts for O_2 reduction: Pt monolayer on carbon-supported PdIr Nanoparticles. *Electrocatalysis* **1,** 213–223 (2010).
61. Xing, Y. *et al.* Enhancing oxygen reduction reaction activity via Pd-Au alloy sublayer mediation of Pt monolayer electrocatalysts. *J. Phys. Chem. Lett.* **1,** 3238–3242 (2010).
62. Wang, J. X. *et al.* Oxygen reduction on well-defined core-shell nanocatalysts: particle size, facet and Pt shell thickness effects. *J. Am. Chem. Soc.* **131,** 17298–17302 (2009).
This is an exemplary paper in a long series by the Adzic group developing core–shell nanoparticle catalysts having Pt monolayer skins, controlled size and surface facets.
63. Gong, K., Su, D. & Adzic, R. Platinum-monolayer shell on $AuNi_{0.5}Fe$ nanoparticle core electrocatalyst with high activity and stability for the oxygen reduction reaction. *J. Am. Chem. Soc.* **132,** 14364–14366 (2010).
64. Ball, S. *et al.* Structure and activity of novel Pt core-shell catalysts for the oxygen reduction reaction. *ECS Trans.* **25,** 1023–1036 (2009).
65. Korovina, A., Garsany, Y., Epshteyn, A., Swider-Lyons, K. E. & Ramaker, D. E. Insight into oxygen reduction on platinum-tantalum oxyphosphate electrocatalysts. *218th ECS Meeting* abstr. 687 (The Electrochemical Society, 2010).
66. Park, S. *et al.* Polarization losses under accelerated stress test using multiwalled carbon nanotube supported Pt catalyst in PEM fuel cells. *J. Electrochem. Soc.* **158,** B297–B302 (2011).
67. Wang, X., Waje, M. & Yan, Y. CNT-based electrodes with high efficiency for PEMFCs. *Electrochem. Solid-State Lett.* **8,** A42–A44 (2005).
68. Chen, Z., Waje, M., Li, W. & Yan, Y. Supportless Pt and PtPd nanotubes as electrocatalysts for oxygen-reduction reactions. *Angew. Chem. Int. Edn* **46,** 4060–4063 (2007).
69. van der Vliet, D. *et al.* Metallic nanotubes with tunable composition and structure as advanced electrocatalysts. *Nature Mater.* (submitted).
70. Zhou, H., Zhou, W.-P., Adzic, R. & Wong, S. S. Enhanced electrocatalytic performance of one-dimensional metal nanowires and arrays generated via an ambient surfactantless synthesis. *J. Phys. Chem. C* **113,** 5460–5466 (2009).
71. Adzic, R. Contiguous platinum monolayer oxygen reduction electrocatalysts on high-stability-low-cost supports. In *2011 DOE Hydrogen Program Annual Merit Review* FC-009, http://www.hydrogen.energy.gov/pdfs/review11/fc009_adzic_2011_o.pdf (2011).
72. Shao, M. Palladium-based electrocatalysts for hydrogen oxidation and oxygen reduction reactions. *J. Power Sources* **196,** 2433–2444 (2011).
73. Myers, D. Non-platinum bimetallic cathode electrocatalysts. In *2008–2010 DOE Hydrogen Program Annual Merit Reviews* http://www.hydrogen.energy.gov/pdfs/review10/fc004_myers_2010_o_web.pdf (2010).
74. Atanasoski, R. & Dodelet, J.-P. in *Encyclopedia of Electrochemical Power Sources* (eds Garche, J. *et al.*) Vol. 2 639–649 (Elsevier, 2009).
75. Lei, M., Li, P. G., Li, L. H. & Tang, W. H. A highly ordered Fe-N-C nanoarray as a non-precious oxygen-reduction catalyst for proton exchange membrane fuel cells. *J. Power Sources* **196,** 3548–3552 (2011).
76. Wang, S., Yu, D. & Dai, L. Polyelectrolyte functionalized carbon nanotubes as efficient metal-free electrocatalysts for oxygen reduction. *J. Am. Chem. Soc.* **133,** 5182–5185 (2011).
77. Zelenay, P. Advanced cathode catalysts. In *2010 DOE Hydrogen Program Annual Merit Review*, http://www.hydrogen.energy.gov/pdfs/review10/fc005_zelenay_2010_o_web.pdf (2010).
78. Ishihara, A., Ohgi, Y., Matsuzawa, K., Mitsushima, S. & Ota, K. Progress in non-precious metal oxide-based cathode for polymer electrolyte fuel cells. *Electrochim. Acta* **55,** 8005–8012 (2010).
79. Lefevre, M., Proietti, E., Jaouen, F. & Dodelet, J.-P. Iron-based catalysts with improved oxygen reduction activity in polymer electrolyte fuel cells. *Science* **324,** 71–74 (2009).
80. Bashyam, R. & Zelenay, P. A class of non-precious metal composite catalysts for fuel cells. *Nature* **443,** 63–66 (2006).
81. Proietti, E. *et al.* Iron-based cathode catalyst with enhanced power density in polymer electrolyte membrane fuel cells. *Nature Commun.* **2,** 416 (2011).
This paper is the latest in a long series by these authors that show an amazing rate of improvement in non-precious metal catalysts' beginning-of-life performances under pure oxygen.
82. Wood, T. E., Tan, Z., Schmoeckel, A. K., O'Neill, D. & Atanasoski, R. Non-precious metal oxygen reduction catalyst for PEM fuel cells based on nitroaniline precursor. *J. Power Sources* **178,** 510–516 (2008).
83. Wu, G., More, K. L., Johnston, C. M. & Zelenay, P. High-Performance electrocatalysts for oxygen reduction derived from polyaniline, iron and cobalt. *Science* **332,** 443–447 (2011).
84. Global *and China Low-E Glass Industry Report* http://pressexposure.com/Global_and_China_Low-E_Glass_Industry_Report,_2010_-_Published_by_ResearchInChina-205310.html (ResearchInChina, 2010).
85. Chen, S., Gasteiger, H. A., Hayakawa, K., Tada, T. & Shao-Horn, Y. Platinum-alloy cathode catalyst degradation in proton exchange membrane fuel cells: nanometer-scale compositional and morphological changes. *J. Electrochem. Soc.* **157,** A82–A97 (2010).
86. Kongkanand, A., Liu, Z., Dutta, I. & Wagner, F. T. Electrochemical and microstructural evaluation of aged nanostructured thin film fuel cell electrocatalyst. *J. Electrochem. Soc.* **158,** B1286–B1291 (2011).
87. Wagner, F. T. *et al.* Catalyst development needs and pathways for automotive PEM fuel cells. *ECS Trans.* **3,** 19 (2006).
88. Koh, S., Hahn, N., Yu, C. & Strasser, P. Effects of composition and annealing conditions on catalytic activities of dealloyed Pt-Cu nanoparticle electrocatalysts for PEMFC. *J. Electrochem. Soc.* **155,** B1281–B1288 (2008).
89. Oezaslan, M., Hasche, F. & Strasser, P. Structure-activity relationship of dealloyed $PtCo_3$ and $PtCu_3$ nanoparticle electrocatalyst for oxygen reduction reaction in PEMFC. *ECS Trans.* **33,** 333–341 (2010).
90. Strasser, P., Hahn, N. T. & Koh, S. Corrosion and ORR activity of Pt alloy electrocatalysts during voltammetric pretreatment. *ECS Trans.* **3,** 139–149 (2006).
91. Mani, P., Srivastava, R. & Strasser, P. Dealloyed binary PtM_3 (M = Cu, Co, Ni) and ternary $PtNi_3M$ (M = Cu, Co, Fe, Cr) electrocatalysts for the oxygen reduction reaction: performance in polymer electrolyte membrane fuel cells. *J. Power Sources* **196,** 666–673 (2011).
92. Neyerlin, K. C., Srivastava, R., Yu, C. & Strasser, P. Electrochemical activity and stability of dealloyed Pt-Cu and Pt-Cu-Co electrocatalysts for the oxygen reduction reaction (ORR). *J. Power Sources* **186,** 261–267 (2009).
93. Wagner, F. T. High-activity dealloyed catalysts. *2011 DOE Hydrogen Program Annual Merit Review* FC-087, http://www.hydrogen.energy.gov/pdfs/review11/fc087_wagner_2011_o.pdf (2011).

94. Strasser, P. *et al.* Lattice-strain control of the activity in dealloyed core-shell fuel cell catalysts. *Nature Chem.* **2,** 454–460 (2010).
95. Snyder, J., Fujita, T., Chen, M. W. & Erlebacher, J. Oxygen reduction in nanoporous metal-ionic liquid composite electrocatalysts. *Nature Mater.* **9,** 904–907 (2010).
This paper shows that porosity on the nanometre scale can be controlled in Ni/Pt alloys, describes the spontaneous formation of core/shell catalysts during de-alloying and illustrates a new concept for enhancing the activity of solid surfaces in contact with ionic liquids.
96. Erlebacher, J. & Seshardi, R. Hard materials with tunable porosity. *MRS Bull.* **34,** 561–568 (2009).
97. Snyder, J. & Erlebacher, J. The active surface area of nanoporous metals during oxygen reduction. *ECS Trans.* **41,** 1021–1030 (2011).

Acknowledgements I gratefully acknowledge support by the Fuel Cell Technologies Program in the Office of Energy Efficiency and Renewable Energy at the US Department of Energy, for grant DE-FG36-07GO17007.

Author Information Reprints and permissions information is available at www.nature.com/reprints. The author declares no competing financial interests. Readers are welcome to comment on the online version of this article at www.nature.com/nature. Correspondence and requests for materials should be addressed to the author (mkdebe1@mmm.com).